17th Australasian Fluid Mechanics Conference
Auckland, New Zealand
5-9 December 2010

High fidelity measurements of fully developed turbulent flow in pipes and channels

J. P. Monty, H. C. H. Ng, N. Hutchins, M. S. Chong and I. Marusic

Department of Mechanical Engineering
The University of Melbourne, VIC 3010, Australia

Abstract

Single, normal hot-wire measurements of the streamwise velocity, u, of a fully developed, turbulent channel and pipe flow for friction Reynolds numbers up to $Re_\tau = 3000$ are presented. Measurement spatial resoluiton was held constant by maintaining a viscous scaled sensor length of $l^+ \approx 22$ ($= lU_\tau/\nu$ where l is wire length, U_τ is friction velocity and ν is the kinematic viscosity).

Introduction

A recent study of hot-wire anemometry has provided new guidance in achieving highly accurate measurements in wall-turbulence [7]. This has made possible the identificaton of sensor-induced inaccuracies, permitting a better understanding of published data and its perceived inconsistenicies. This paper documents the application of these new 'guidelines' to best-practice hot-wire anemometry, providing the most accurate database of streamwise velocity in fully developed, turbulent pipe and channel flows. All experiments were performed in facilities at Melbourne [17]. These measurements will not only improve the fundamental understanding of wall-turbulence, but also provide a much-needed database for the validation of Direct Numerical Simulation (DNS) studies of these flows.

Apparatus

Facilities

The channel flow facility is a blower type facility with a working section length of 22m and a cross-section measuring 1170×100mm. The $11.7:1$ width-to-height ratio ensures two-dimensionality of the flow and the long working section ensures that the flow is fully developed. Further details of this flow facility can be found in [18]. The pipe flow facility is a suction type facility and has a diameter of $D = 98.8$mm and a working section length of $L = 38.86$m. This corresponds to a pipe length-to-diameter ratio of $L/D = 393.4$ ensuring that the flow is fully developed. Full details of this facility are available in [21]. In both facilities, the friction velocity U_τ, is determined by measuring the static pressure gradient. Importantly, these facilities have a nominally equivalent outer length scale, channel half-height $h = 50.0$mm and pipe radius, $R = 49.4$mm, and each has a maximum centreline velocity of approximately $U_{cl} \approx 35$m/s. This allows a convenient comparison of results obtained from each of these facilities.

Anemometry details

In order to maintain a hot-wire length-to-diameter ratio of $l/d \geq 200$ as recommended by [10], hot-wire diameters required for this study ranged from 1.5μm to 5.0μm. The hot-wires were constructed using *Dantec 55P05* and *55P15* boundary-layer type probes with a tip spacing of 3mm (for 5μm wires) and 1.25mm (for 1.5μm and 2.5μm wires) respectively. Having soldered the wires onto the probe tips, the sensing elements are carefully etched to pre-determined lengths to satisfy the matched $l^+ = 22$ criterion. All hot-wire probes are operated in constant temperature mode using a custom built Melbourne University Constant Temperature Anemometer (MUCTA II). The anemometer was operated at an overheat ratio of 1.8. The system frequency response to a $1kHz$ square wave was set to a frequency corresponding to $t^+ = tU_\tau^2/\nu \leq 1$. This equated to greater than 75kHz at the highest Reynolds number tested.

The hot-wire probes are calibrated *in situ* against a Pitot-static probe for both facilities. Calibration of the hot-wire sensors in the pipe flow were also carried out *in situ*. The pipe test section is removed, the hot-wire is aligned and the initial wall normal position is determined by a microscope. The pitot probe is offset from the hot-wire probe in the wall normal direction. The offset of the two sensors is measured before the test section is placed back into the facility. Since the mean velocity profile of the pipe flow is symmetrical and the velocity gradients are shallow in the core of the flow, hot-wire calibration can be carried out by ensuring the hot-wire and Pitot-tube anemometers are placed equidistant about the pipe centreline. For the channel facility, the calibration is carried out at the channel centre-line or channel half-height where turbulence intensities are at a minimum. The Pitot probe and hot-wire are aligned in an external rig to have the same wall normal position, and the probes are offset in the spanwise direction by 10mm. The hot-wire is aligned to be parallel to the wall and the initial wall normal location of the hot-wire is measured using a microscope. For all measurements, a *Renishaw* linear optical encoder with 0.5μm resolution is used to determine the location of the probe relative to the initial wall normal location. The encoder is used throughout the traversing measurement and hot-wire calibration procedure.

For all experiments, an *MKS Baratron* pressure transducer and *MKS Type 270* signal conditioner are used to measure the pressures from the Pitot-static probe during calibration and the traversing measurements as well as measuring the static pressure gradient in the flow facility. The temperature and atmospheric pressure were measured using a calibrated thermocouple and a *Sensortechnics* 144S-BARO barometer. All signals were sampled using a *Data Translation* DT-9836 16-bit data acquisition board. hot-wire signals were sampled at an interval of $\Delta t^+ \leq 0.5$ to ensure that smallest energetic scales are captured. Full details of the experimental conditions and sensor parameters are provided in table 1.

Results

Mean statistics

Figures 1(a) and 1(c) are channel flow mean velocity and turbulence intensity profiles and figure 1(b) and 1(d) are the corresponding pipe flow profiles. The channel flow data presented here was found to be in good agreement with a logarithmic law of the wall with constants $\kappa = 0.39$ and $A = 4.42$ and the pipe flow data agreed to constants $\kappa = 0.38$ and $A = 4.23$ (although

Facility	U_{cl}	Re_τ	d(μm)	l(mm)	l^+	l/d	Δt^+	f_s(kHz)	T(s)	TU_{cl}/δ
Channel	7.430	1053	5.0	1.040	21.9	208	0.07	100	150	22290
Channel	15.55	2072	2.5	0.538	22.3	216	0.26	100	120	37320
Channel	23.71	3026	1.5	0.346	21.0	231	0.47	120	30	14227
Pipe	7.63	1046	5.0	1.040	22.0	208	0.46	15	120	18525
Pipe	16.35	2002	2.5	0.575	22.4	230	0.43	60	60	19852
Pipe	25.47	2984	1.5	0.366	22.1	244	0.49	120	45	23205

Table 1: Experimental conditions and hot-wire sensor parameters for all experiments.

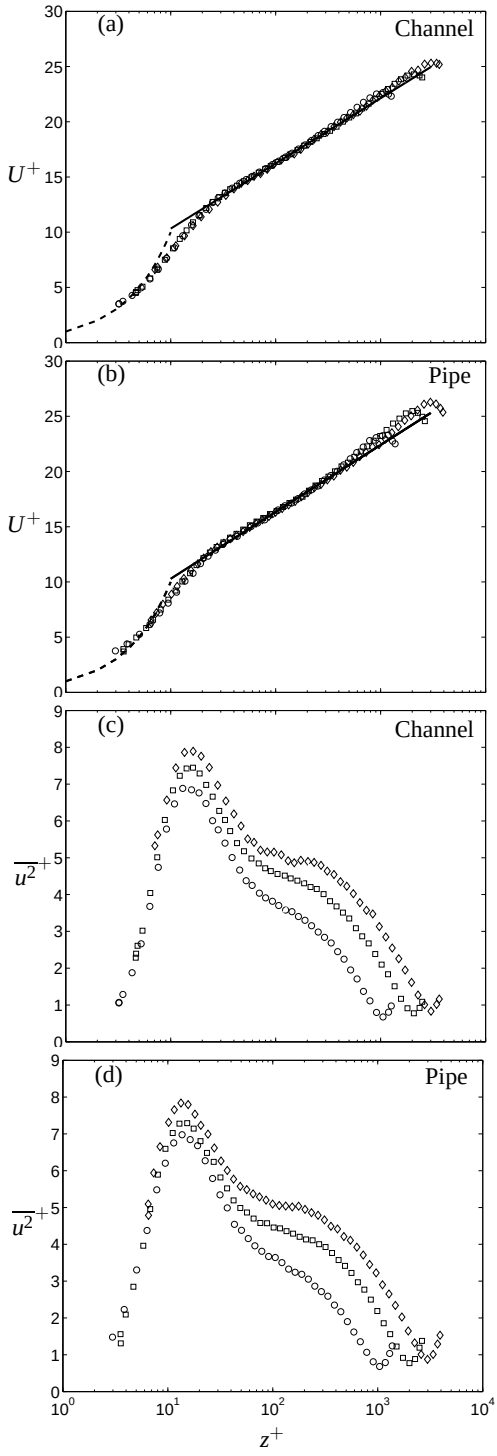

Figure 1: Mean velocity and turbulence intensity profiles of channel flow (a) & (c) and pipe flows (b) & (d) respectively.

either will fit within experimental error in this Reynolds number range). The constants for all measurements were determined by performing a linear regression for all data points that lie within the range $100 \leq z^+ \leq 0.15\delta^+$ ($\delta^+ = \delta U_\tau/\nu = Re_\tau$). The traditional logarithmic law, with 'universal' constants κ and A is defined as,

$$U^+ = \frac{1}{\kappa}\ln(z^+) + A. \quad (1)$$

It must be noted that only a limited logarithmic region exists for all but the highest Reynolds number. Although there exists some ongoing controversy regarding the universality of the log law constants and values vary throughout the literature (see: [12, 15, 19, 20, 22, 23]), the values reported here come from a 'best' fit to the new data only. In viscous scaling, the mean velocity profiles (figures 1(a) and 1(b)) of both geometries exhibit similarity in the near wall and logarithmic regions and only deviate in the outer or wake regions. The deviation from the log law of the wall highlights the different 'wake strength' present in the flow for each geometry. This is consistent with findings in [17], where it was noted that 'wake strength' is strongest for zero-pressure gradient flat plate boundary layer followed by pipes followed by channels.

Figures 1(c) and 1(d) are the streamwise turbulence intensity profiles for channels and pipes respectively. With a constant measurement resolution (matched $l^+ = 22$), the behaviour of the streamwise turbulence intensity is isolated from attenuation due to sensor size. The similarity (at least to within experimental error) between channels and pipes for $1000 \leq Re_\tau \leq 3000$ across the entire layer is consistent with [17] where similarity between channel, pipe and boundary layers was examined for a single Reynolds number of $Re_\tau = 3000$. Furthermore, it appears that the near-wall peak in turbulence intensity, $\overline{u^2}^+|_m$ (where m denotes the peak or maximum) grows with Reynolds number for both internal geometries. The growth of $\overline{u^2}^+|_m$ is consistent with the DNS channel flow studies of [4] and [8] and is already well established for boundary layers over a range of Reynolds numbers spanning laboratory to atmospheric scale flows. (see : [2, 3, 11, 16]). The recent experimental investigation of [7] reports a similar trend in boundary layers for similarly well resolved hot-wire measurements ($l^+ \approx 22$), albeit at higher Reynolds numbers ($2800 \leq Re_\tau \leq 19000$). However, higher Reynolds number studies in turbulent duct flows with constant measurement resolution would be required to confirm the Reynolds number dependence of $\overline{u^2}^+|_m$ because within the range of Reynolds numbers here, the rise in the near wall peak falls approximately within a $\pm 4\%$ range or almost within the error range of hot-wire measured turbulence intensity.

Energy spectra

Iso-contours of the pre-multiplied u spectra as a function of

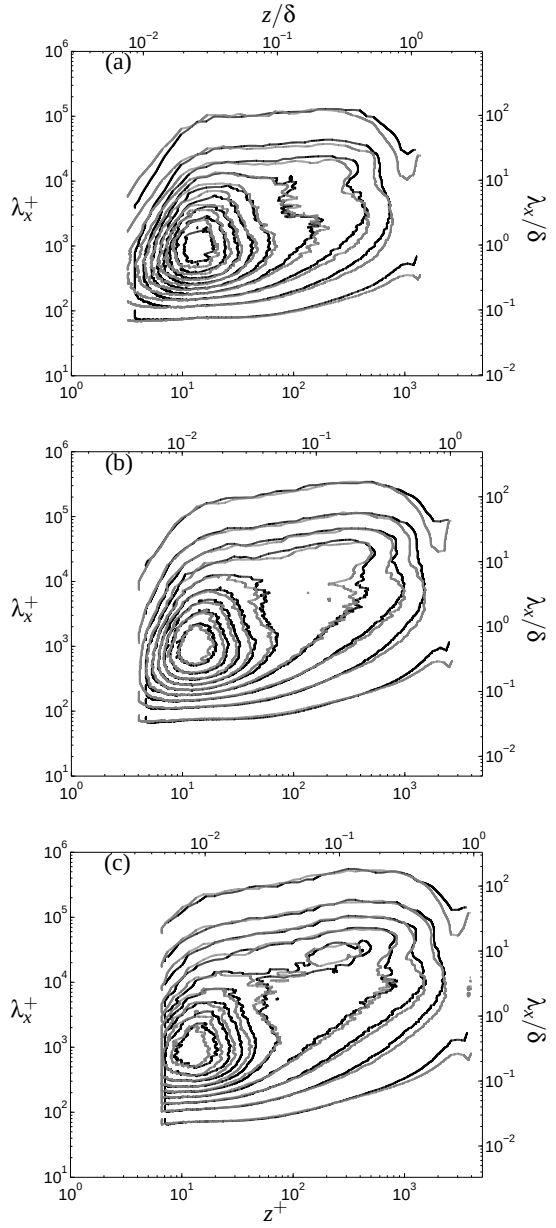

Figure 2: Contours of u spectra for (a) $Re_\tau = 1000$, (b) $Re_\tau = 2000$ and (c) $Re_\tau = 3000$. Channel (black), pipe (grey). $k_x\phi_{uu}/U_\tau^2$, contour levels $[0.1 : 0.2 : 1.7]$.

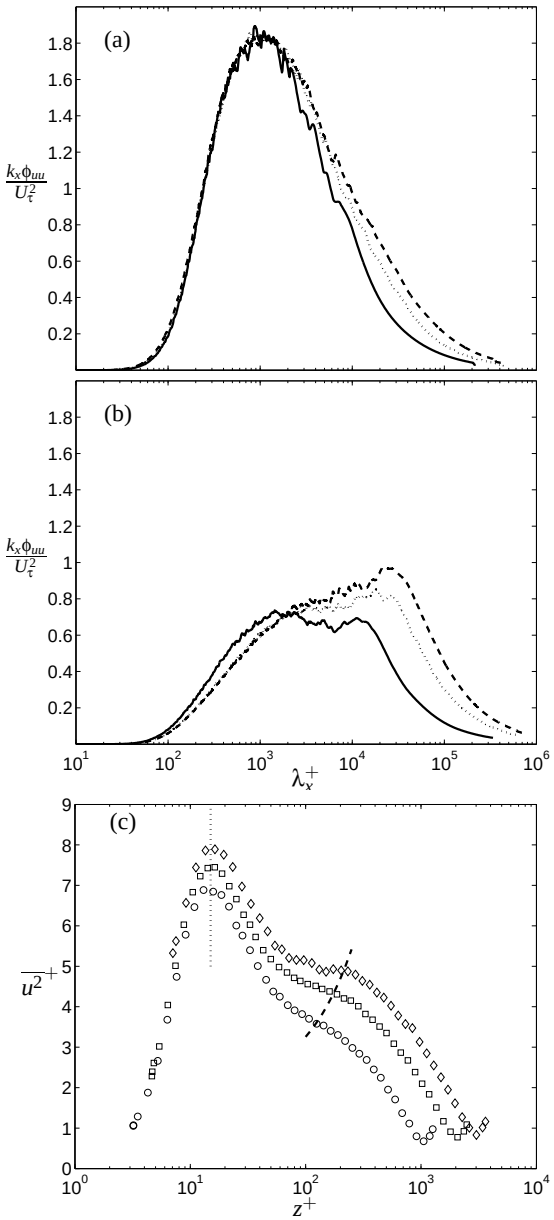

Figure 3: Channel flow spectra for $Re_\tau = 1000$, 2000 and 3000, at : (a) $z^+ = 15$ and (b) $z+ = 3.9\sqrt{Re_\tau}$. (c) Channel flow turbulence intensity profile: $(\cdots)$ $z^+ = 15$, $(--)$ $z^+ = 3.9\sqrt{Re_\tau}$.

streamwise wavelength (λ_x^+ or λ_x/δ) and wall normal position (z^+ or z/δ) are plotted together for comparison in figure 2, with plots (a), (b) and (c) corresponding to $Re_\tau = 1000$, 2000 and 3000 respectively. The nominally equivalent outer length scale allows data to be simultaneously presented in both viscous and outer scaling. Clearly, the channel and pipe flow u spectra are very similar in energy content and distribution being effectively the same within experimental uncertainty. Generally, the duct flows have been shown to possess three predominant energetic modes. One mode is at a fixed position with viscous scaling ($z^+ \approx 15$, $\lambda_x^+ \approx 1000$) and a fixed magnitude for a given wire length l^+, and represents the energy contribution of the near wall cycle. [9] identified two other modes that exist in the logarithmic region and beyond for pipe flows. These other modes were shown to scale on δ and appear at wavelengths of $\lambda_x \approx 1-3\delta$ and $\lambda_x \approx 12-14\delta$ and are the Large-scale motions (LSM) and Very-large-scale motions (VLSM) respectively. The LSM and VLSM were also shown to exist in channel flows by [1] and [18] among others. In contrast, [6] show only a single energetic peak at $\lambda_x \approx 6\delta$ for boundary layer flows and also noted that the bi-modal distribution of the boundary layer u spectrum is not as apparent at low Reynolds numbers due to an insufficient scale separation and a short logarithmic overlap region. However, it was noted by [5] and [17] that the boundary layer spectra does seem to settle to a peak with $\lambda_x \approx 2-3\delta$ in the outer wake region of the flow.

Structure in the near wall and log regions

Figure 3(a) and 3(b) are plots of the u spectra from channel flow at $z^+ \approx 15$ and the geometric midpoint of the log region, $z^+ = 3.9\sqrt{Re_\tau}$ (see : [13, 14]), respectively. These wall normal locations are marked with dashed lines on the turbulence intensity profiles of figure 3(a). At $z^+ \approx 15$, the u spectra collapses well in the small scales and reveals an increasing contribution from the large scales. Since the integrated area

under the pre-multiplied spectra is equivalent to the turbulence intensity, $\overline{u^2}^+$, it is the contribution of the large scales that is responsible for the rise in $\overline{u^2}^+|_m$. Similarly, it can be seen in figure 3(b) that the increasing large scale contribution causes the rise in $\overline{u^2}^+$ in the log region. However, the spectra no longer collapse in the small scales. At $Re_\tau = 1000$, the signature of the near wall cycle is still apparent and manifests itself as a hump at the small-scale end. This is likely due to the lack of scale seperation. At $Re_\tau = 2000$ and 3000, however, the energy is dominated by large scale motions and a prominent hump at $\lambda_x^+ = 1000$ is absent. For all three Reynolds numbers, the growing contribution of the outer peak is clear. This outer peak is the energy signature of the VLSM which is fixed in outer scaled wavelengths at $10 \leq \lambda_x/\delta \leq 20$.

Conclusions

From new measurements of streamwise velocity in turbulent channel and pipe flows for Reynolds numbers $1000 \leq Re_\tau \leq 3000$ and a matched viscous scaled wire length of $l^+ = 22$, it was shown that turbulent channel and pipe flows have similar mean velocity profiles, turbulence intensity profiles and energy spectra. The only discrepancy is that pipe flows consistently exhibit a stronger wake, observed as a larger deviation from the log law of the wall when compared to channels. The u spectra and turbulence intensity profiles are similar across the entire layer. The constant measurement resolution allows a direct comparison across the flows and it can be seen that the near wall peak in turbulence intensity $\overline{u^2}^+$ is Reynolds number dependent for the range of Reynolds numbers investigated here. With DNS data for channel flows currently available up to $Re_\tau = 2000$, the data presented here may serve as a timely database for comparison between numerical and physical experiments.

Acknowledgements

The authors wish to gratefully acknowledge the financial support of the Australian Research Council.

References

[1] Balakumar, B. J. and Adrian, R. J., Large and very-large-scale motions in channel and boundary-layer flows, *Phil. Trans. R. Soc. A*, **365**, 2007, 665–681.

[2] DeGraaff, D. B. and Eaton, J. K., Reynolds-number scaling of the flat-plate turbulent boundary layer, *Journal of Fluid Mechanics*, **422**, 2000, 319–346.

[3] Fernholz, H. H. and Finley, P. J., The incompressible zero-pressure-gradient turbulent boundary layer : An assessment of the data, *Prog. Aerospace Sci.*, **32**, 1996, 245–311.

[4] Hoyas, S. and Jiménez, J., Scaling of velocity fluctuations in turbulent channel flows up to $Re_\tau = 2003$, *Physics of Fluids*, **18**.

[5] Hutchins, N. and Marusic, I., Evidence of very long meandering features in the logarithmic region of turbulent boundary layers, *Journal of Fluid Mechanics*, **579**, 2007, 1–28.

[6] Hutchins, N. and Marusic, I., Large-scale influences in near-wall turbulence, *Phil. Trans. R. Soc. A*, **365**, 2007, 647–664.

[7] Hutchins, N., Nickels, T., Marusic, I. and Chong, M., Hot-wire spatial resolution issues in wall-bounded turbulence, *Journal of Fluid Mechanics*, **635**, 2009, 103–136.

[8] Jiménez, J. and Hoyas, S., Turbulent fluctuations above the buffer layer of wall-bounded turbulence, *Journal of Fluid Mechanics*, **611**, 2008, 215–236.

[9] Kim, K. C. and Adrian, R. J., Very large-scale motion in the outer layer, *Physics of Fluids*, **11**, 1999, 417–422.

[10] Ligrani, P. and Bradshaw, P., Spatial resolution and measurement of turbulence in the viscous sublayer using subminiature hot-wire probes, *Experiments in Fluids*, **5**, 1987, 407–417.

[11] Marusic, I. and Kunkel, G. J., Streamwise turbulence intensity formulation for flat plat-plate boundary layers, *Physics of Fluids*, **15**, 2003, 2461–2464.

[12] Marusic, I., McKeon, B. J., Monkewitz, P. A., Nagib, H. M., Smits, A. J. and Sreenivasan, K. R., Wall-bounded turbulent flows at high Reynolds numbers: Recent advances and key issues, *Physics of Fluids*, **22**.

[13] Mathis, R., Hutchins, N. and Marusic, I., Large-scale amplitude modulation of the small-scale structures in turbulent boundary layers, *Journal of Fluid Mechanics*, **628**.

[14] Mathis, R., Monty, J., Hutchins, N. and Marusic, I., Comparison of large-scale amplitude modulation in boundary layers, pipes and channel flows, *Physics of Fluids*, **21**, 2009, 311–337.

[15] McKeon, B. J., Li, J., Jiang, W., Morrison, J. F. and Smits, A. J., Further observations on the mean velocity distribution in fully developed pipe flow, *Journal of Fluid Mechanics*, **501**, 2004, 135–147.

[16] Metzger, M. and Klewicki, J., A comparative study of near-wall turbulence in high and low Reynolds number boundary layers, *Physics of Fluids*, **13**, 2001, 692–701.

[17] Monty, J. P., Hutchins, N., Ng, H., Marusic, I. and Chong, M. S., A comparison of turbulent pipe, channel and boundary layer flows, *Journal of Fluid Mechanics*, **632**, 2009, 431–442.

[18] Monty, J. P., Stewart, J. A., Williams, R. C. and Chong, M. S., Large-scale features in turbulent pipe and channel flows, *Journal of Fluid Mechanics*, **589**, 2007, 147–156.

[19] Nagib, H. M. and Chauhan, K., Variations of von Kármán coefficient in canonical flows, *Physics of Fluids*, **20**.

[20] Perry, A. E., Hafez, S. and Chong, M. S., A possible reinterpretation of the princeton superpipe data, *Journal of Fluid Mechanics*, **439**, 2001, 395–401.

[21] Perry, A. E., Henbest, S. and Chong, M. S., A theoretical and experimental study of wall turbulence, *Journal of Fluid Mechanics*, **165**, 1986, 163–199.

[22] Zagarola, M. and Smits, A., Mean flow scaling in turbulent pipe flow, *Journal of Fluid Mechanics*, **373**, 1998, 33–79.

[23] Zanoun, E. S., Durst, F. and Nagib, H., Evaluating the law of the wall in two-dimensional fully developed turbulent channel flows, *Physics of Fluids*, **15**, 2003, 3079–3089.